ATLAS CONF Note

ATLAS-CONF-2017-023

21st March 2017

Angular analysis of $B^0_d \to K^*\mu^+\mu^-$ decays in pp collisions at $\sqrt{s} = 8$ TeV with the ATLAS detector

The ATLAS Collaboration

An angular analysis of the decay $B^0_d \to K^*\mu^+\mu^-$ is presented using proton-proton collisions at $\sqrt{s} = 8$ TeV from LHC data analysed with the ATLAS detector. The study is based on 20.3 fb^{-1} of integrated luminosity collected during 2012. Measurements of the K^* longitudinal polarisation fraction and a set of angular parameters obtained for this decay are presented. The results are compatible with theoretical predictions.

ATLAS-CONF-2017-023
03 April 2017

© 2017 CERN for the benefit of the ATLAS Collaboration.
Reproduction of this article or parts of it is allowed as specified in the CC-BY-4.0 license.

1 Introduction

Flavor changing neutral currents (FCNC) have played a significant role in the construction of the Standard Model of particle physics (SM). These processes are forbidden at tree level. They proceed at next to leading order, via loops, and hence are rare. An important set of FCNC processes involve the transition of a b quark to an $s\mu^+\mu^-$ final state mediated by electroweak box and loop diagrams. The latter topology is sometimes referred to as a penguin contribution. If heavy new particles exist they may contribute to FCNC decay amplitudes, affecting the measurement of observables related to the decay under study. Hence FCNC processes allow to search for contributions from sources of physics beyond the SM (hereafter referred to as new physics). This analysis focuses on the decay $B^0_d \to K^*(892)\mu^+\mu^-$, where $K^*(892) \to K^+\pi^-$. Hereafter the $K^*(892)$ is referred to as K^*, and charge conjugation is implied throughout unless stated otherwise. In addition to angular observables such as the forward-backward asymmetry[1] ($A_{\rm FB}$), there is considerable interest in measurements of the charge asymmetry, differential branching fraction, isospin asymmetry, and ratio of rates of decay to di-muon and di-electron final states, all as a function of the invariant mass squared of the di-lepton system (q^2). All of these observable sets can be sensitive to different types of new physics introduced as FCNCs at tree or loop level. The *BABAR*, Belle, CDF, CMS, and LHCb Collaborations have published the results of studies of the angular distributions for $B^0_d \to K^*\mu^+\mu^-$ [1–7]. The LHCb Collaboration has recently reported a potential hint, at the level of 3.4 standard deviations, for a deviation from SM calculations [3, 4] in this decay mode when using a parameterisation of the angular distribution designed to minimise uncertainties from hadronic form factors. Measurements using this approach have recently been reported by the Belle Collaboration [7] which are consistent with the LHCb experiment's results and with the SM calculations. This paper presents results following the methodology outlined in Ref. [3] and the convention adopted by the LHCb Collaboration for the definition of angles found in Ref. [8].

This article presents the results of an angular analysis of the decay $B^0_d \to K^*\mu^+\mu^-$ with the ATLAS detector, using 20.3 fb^{-1} of pp collision data at a centre of mass energy $\sqrt{s} = 8$ TeV delivered by the Large Hadron Collider (LHC) [9] during 2012. In order to compare with other experiments and phenomenology studies, results are presented in six different bins of q^2 in the range 0.04 to 6.0 GeV^2, where three of these bins overlap. Backgrounds, including a radiative tail from $B^0_d \to K^* J/\psi$ events, increase for q^2 above 6.0 GeV^2. For this reason data above this value are not included.

The operator product expansion used to describe the decay $B^0_d \to K^*\mu^+\mu^-$ encodes short distance contributions in terms of Wilson coefficients and long distance contributions in terms of operators [10]. Global fits for Wilson coefficients have been performed using measurements of $B^0_d \to K^*\mu^+\mu^-$ and other rare processes in the context of understanding the SM and searching for discrepancies that might lead to a deeper understanding of new physics. Those studies aim to identify any consistent patterns of deviation from SM expectations for several decays that might indicate structure of the underlying new physics Lagrangian, see Refs [11, 12]. The parameters presented in this article can be used as inputs to these global fits.

[1] The normalised difference between the number of muons going in the forward and in the backward direction with respect to the opposite B direction in the di-muon rest frame.

2 Analysis method

Three angular variables are used to describe the decay: the angle between the K^+ and the direction opposite to the B^0_d in the K^* centre of mass frame (θ_K); the angle between the μ^+ and the direction opposite to the B^0_d in the di-muon centre of mass frame (θ_L); and the angle between the two decay planes formed by the $K\pi$ and the di-muon systems in the B^0_d rest frame (ϕ). For $\overline{B}{}^0_d$ mesons the definitions are given with respect to the negatively charged particles. Figure 1 illustrates the angles used.

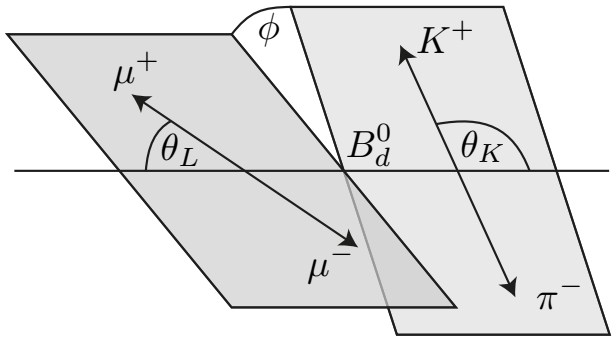

Figure 1: An illustration of the $B^0_d \to K^*\mu^+\mu^-$ decay showing the angles θ_K, θ_L and ϕ defined in the text. Angles are computed in the rest frame of the K^*, di-muon system and B^0_d meson, respectively.

The angular differential decay rate for $B^0_d \to K^*\mu^+\mu^-$ is a function of q^2, $\cos\theta_K$, $\cos\theta_L$ and ϕ, and can be written in several different ways [13]. The form to express the differential decay amplitude as a function of the angular parameters uses coefficients that may be represented by the helicity or transversity amplitudes [14] and is written as[2]

$$\begin{aligned}\frac{1}{\mathrm{d}\Gamma/\mathrm{d}q^2}\frac{\mathrm{d}^4\Gamma}{\mathrm{d}\cos\theta_L\mathrm{d}\cos\theta_K\mathrm{d}\phi\mathrm{d}q^2} &= \frac{9}{32\pi}\Bigg[\frac{3(1-F_L)}{4}\sin^2\theta_K + F_L\cos^2\theta_K + \frac{1-F_L}{4}\sin^2\theta_K\cos 2\theta_L \\ &\quad -F_L\cos^2\theta_K\cos 2\theta_L + S_3\sin^2\theta_K\sin^2\theta_L\cos 2\phi \\ &\quad +S_4\sin 2\theta_K\sin 2\theta_L\cos\phi + S_5\sin 2\theta_K\sin\theta_L\cos\phi \\ &\quad +S_6\sin^2\theta_K\cos\theta_L + S_7\sin 2\theta_K\sin\theta_L\sin\phi \\ &\quad +S_8\sin 2\theta_K\sin 2\theta_L\sin\phi + S_9\sin^2\theta_K\sin^2\theta_L\sin 2\phi\Bigg]. \end{aligned} \quad (1)$$

Here F_L is the fraction of longitudinally polarised K^*'s and the S_i are angular coefficients. These angular parameters are functions of the real and imaginary parts of the transversity amplitudes of B^0_d decays to $K^*\mu^+\mu^-$. The forward-backward asymmetry is given by $A_{\mathrm{FB}} = 3S_6/4$. The S_i parameters depend on hadronic form factors which have significant uncertainties at leading order. It is possible to reduce the theoretical uncertainty on the parameters extracted from data by transforming the S_i using ratios constructed to cancel form factor uncertainties at leading order. These ratios are given by Refs [14, 15]

[2] This equation neglects possible $K\pi$ S-wave contributions. The effect of an S-wave contribution is considered following the method used by LHCb in [3].

as

$$P_1 = \frac{2S_3}{1-F_L} \quad (2)$$

$$P_2 = \frac{2}{3}\frac{A_{\rm FB}}{1-F_L} \quad (3)$$

$$P_3 = -\frac{S_9}{1-F_L} \quad (4)$$

$$P'_{i=4,5,6,8} = \frac{S_{j=4,5,7,8}}{\sqrt{F_L(1-F_L)}}. \quad (5)$$

All of the parameters introduced, F_L, S_i and $P_i^{(\prime)}$, vary with q^2 and the data are analysed in q^2 bins to obtain an average value for a given parameter in that bin. Measurements of these quantities can be used as inputs to global fits used to determine the values of Wilson coefficients and search for new physics.

3 The ATLAS detector, data, and Monte Carlo samples

The LHC collides bunches of protons in the vacuum of the beam pipe at the interaction point of the ATLAS experiment. The ATLAS detector, as described in Ref. [16], consists of an inner detector (ID), a calorimeter system and a muon spectrometer (MS). The ID consists of silicon pixel and strip detectors, with a straw tube tracker providing additional information for tracks passing through the central region of the detector[3] . The ID has a coverage of $|\eta| < 2.5$, and is immersed in a 2T axial magnetic field generated using a superconducting solenoid. A calorimeter system, consisting of liquid argon and scintillating-tile sampling calorimeter sub-systems, surrounds the ID. The outermost part of the detector is the MS system, which employs several different detector technologies in order to provide muon identification and a muon trigger. A toroidal magnet system is embedded in the MS. The ID, calorimeter and MS systems have full azimuthal coverage.

The data analysed here were recorded in 2012 during the latter part of Run 1 of the LHC. The collision energy of the pp system was $\sqrt{s} = 8$ TeV. After applying beam, detector and data-quality criteria, the data sample analysed comprises of an integrated luminosity of 20.3 fb^{-1}. A number of Monte Carlo (MC) simulated event samples, generated using Pythia 8 [17] and EvtGen [18], with final state radiation simulated using PHOTOS [19] are used. Simulated events are passed through the Geant 4 [20, 21] based ATLAS MC simulation programme and fed through the same reconstruction chain as data. These are studied in order to finalise event selection and explore potential backgrounds. The MC simulation includes modeling of multiple interactions per pp bunch crossing in the LHC. The samples of MC generated events used are described further in Section 5.

[3] ATLAS uses a right-handed coordinate system with its origin at the nominal interaction point (IP) in the centre of the detector and the z-axis along the beam pipe. The x-axis points from the IP to the centre of the LHC ring, and the y-axis points upward. Cylindrical coordinates (r, Φ) are used in the transverse plane, Φ being the azimuthal angle around the z-axis. The pseudorapidity is defined in terms of the polar angle θ as $\eta = -\ln\tan(\theta/2)$.

4 Event selection

Events satisfy a trigger that requires one, two, or more muons. Several trigger signatures constructed from the MS inputs are combined based on availability during the data taking period, prescale factor and efficiency for signal identification. Data are combined from 15 trigger chains where 21%, 89% or 5% of selected events pass at least one trigger with one, two, or at least three muons identified online in the MS, respectively. Of the events passing the trigger, 86% are required to have at least two muons identified at trigger level and the dominant single contribution comes from the requirement of one muon with a transverse momentum $p_{\mathrm{T}} > 4$ GeV and the other muon with $p_{\mathrm{T}} > 6$ GeV. This combination of triggers ensures that the analysis remains sensitive to events down to the kinematic threshold of $q^2 = 4m_\mu^2$, where m_μ is the muon mass. The effective average trigger efficiency for selected signal events corresponds to about 29%.

Muon tracks are formed offline by combining information from both the ID and MS [22]. Tracks are required to satisfy $|\eta| < 2.5$. Candidate muon (kaon and pion) tracks are required to satisfy $p_{\mathrm{T}} > 3.5$ (0.5) GeV. Pairs of oppositely charged muons are required to originate from a common vertex with a $\chi^2 < 10$.

Candidate K^* mesons are formed using pairs of oppositely charged kaon and pion candidates reconstructed from hits in the ID. Candidates are required to satisfy $p_{\mathrm{T}}(K^*) > 3.0$ GeV. As the ATLAS detector does not have a dedicated charged particle identification system, candidates are reconstructed to satisfy both possible $K\pi$ mass hypotheses and the selection relies on the kinematics of the reconstructed K^* meson to determine which of the two tracks corresponds to the kaon. The invariant $K\pi$ mass is required to lie in a window of twice the natural width around the nominal mass of 896 MeV, i.e. in the range [846, 946] MeV. The charge of the kaon candidate is used to assign the flavor of the reconstructed B candidate.

B candidates are reconstructed from a K^* candidate and a pair of oppositely charged muons. The four-track vertex is fitted and required to satisfy $\chi^2 < 2$ to suppress background. A significant amount of combinatorial, B_d^0, B^+, B_s^0 and Λ_b background contamination remains at this stage. Combinatorial background is suppressed by requiring a B_d^0 candidate lifetime significance $\tau/\sigma_\tau > 12.5$, where the decay time uncertainty σ_τ is calculated from the covariance matrices associated with the four-track vertex fit and with the primary vertex fit. Background from partially reconstructed decays exists below the B_d^0 mass and feeds up into the signal region. This contribution is suppressed by requiring an asymmetric mass cut around the nominal B_d^0 mass, $5150 < m_{K\pi\mu\mu} < 5700$ MeV. The high mass sideband is retained as the parameter values for the combinatoric background shapes are extracted from the fit to data described in Section 5. To further suppress background it is required that the angle, Θ, defined between the vector from the primary vertex to the B_d^0 candidate decay vertex and the B_d^0 candidate momentum, satisfies $\cos\Theta > 0.999$. Resolution effects on $\cos\theta_K$, $\cos\theta_L$ and ϕ are found to have a negligible effect on the ATLAS $B_s^0 \to J/\psi\phi$ analysis [23] It is assumed to also be the case for $B_d^0 \to K^*\mu^+\mu^-$.

On average 12%, 2-10%, and 17% of events in the data, exclusive background, and signal MC have more than one candidate reconstructed, respectively. A two-step selection process is used for events containing more than one candidate. The majority, about 96%, of multiple candidates arise from degenerate four track combinations where the kaon and pion assignments are ambiguous. The B_d^0 candidate reconstructed with smallest value of $|m_{K\pi} - m_{K^*}|/\sigma(m_{K\pi})$ is retained for analysis, where $m_{K\pi}$ is the K^* candidate mass, $\sigma(m_{K\pi})$ is the error on this quantity, and m_{K^*} is the world average value of the K^* mass. For the remaining 4% of events, the candidate with the smallest value of the B vertex χ^2 is retained for subsequent analysis. This procedure results in an incorrect flavor tag (mistag) for some signal events. The mistag

probability of a B^0_d ($\overline{B}^0_d$) meson is denoted as ω ($\overline{\omega}$) and is determined from MC simulated events to be 0.1088 ± 0.0005 (0.1086 ± 0.0005). The mistag probability varies slightly with q^2 such that the difference $\omega - \overline{\omega}$ remains consistent with zero. Hence the average mistag rate $\langle\omega\rangle$ in a given q^2 bin is used to account for this effect. If a candidate is mistagged then the values of θ_K and ϕ change sign. Sign changes in these angles affect the overall sign of the terms multiplied by the coefficients S_4, S_5 and S_9 (similarly for the corresponding $P^{(\prime)}$ parameters) in Equation (1). The corollary is that mistagged events result in a dilution factor of $(1 - 2\langle\omega\rangle)$ for the affected coefficients.

The region $q^2 \in [0.98, 1.1]$ GeV^2 is vetoed to remove any potential contamination from the $\phi(1020)$ resonance. The remaining data with $q^2 \in [0.04, 6.0]$ GeV^2 are analysed in order to extract the signal parameters of interest. Two $K^* c\overline{c}$ control sample regions are defined for B decays to $K^* J/\psi$ and $K^*\psi(2S)$, respectively as $q^2 \in [8, 11]$ and $[12, 15]$ GeV^2. The control samples are used to extract nuisance parameters of the signal probability density function (p.d.f.) from data as discussed in Section 5.3.

For $q^2 < 6$ GeV^2 the selected data sample consists of 787 events and is composed of signal $B^0_d \to K^*\mu^+\mu^-$ decay events as well as background that is dominated by a combinatorial component that does not peak in $m_{K\pi\mu\mu}$ and does not exhibit resonant structure in q^2. Other background contributions are considered when computing systematic uncertainties. Above 6 GeV^2 several backgrounds pass the selection imposed, including events coming from the low mass tail of $B \to K^* J/\psi$. Scalar $K\pi$ contributions are neglected in the nominal fit and considered only when addressing systematic uncertainties. The data are analysed in the q^2 bins $[0.04, 2.0]$, $[2.0, 4.0]$, $[4.0, 6.0]$, $[0.04, 4.0]$, $[1.1, 6.0]$, $[0.04, 6.0]$ GeV^2, where the bin width is chosen to provide a sample of signal events sufficient to perform an angular analysis. The width is much larger than the resolution obtained from MC simulated signal events and than observed in data for B^0_d decays to $K^* J/\psi$ and $K^*\psi(2S)$ decays. The overlapping regions are analysed in order to facilitate comparison with other experiments and theory.

5 Maximum likelihood fit

Extended unbinned maximum likelihood fits of the angular distributions of the signal decay are performed on the data for each q^2 bin. The discriminating variables used in the fit are $m_{K\pi\mu\mu}$, the cosines of the helicity angles ($\cos\theta_K$ and $\cos\theta_L$), and ϕ. The likelihood $\mathcal{L}$ for a given q^2 bin is

$$\mathcal{L} = \frac{e^{-N}}{n!} \prod_{i=1}^{n} \sum_j n_j P_{ij}(m_{K\pi\mu\mu}, \cos\theta_K, \cos\theta_L, \phi; \widehat{p}, \widehat{\theta}), \tag{6}$$

where n is the total number of events, the sum runs over signal and background components, n_j is the fitted yield for the j^{th} component, N is the sum over n_j, and P_{ij} is the p.d.f. evaluated for event i and component j. For the nominal fit $j = 2$, as only one background component is considered. The $\widehat{p}$ are parameters of interest (F_L, S_i) and $\widehat{\theta}$ are nuisance parameters. The remainder of this section discusses the signal model (Section 5.1), treatment of background (Section 5.2), use of $K^* c\overline{c}$ decay regions in data (Section 5.3), fitting procedure and validation (Section 5.4).

5.1 Signal model

The signal mass distribution is modeled by a Gaussian distribution where the width σ of the Gaussian is scaled by the per-event uncertainty on the $K\pi\mu\mu$ mass, $\sigma(m_{K\pi\mu\mu})$, i.e. the width is given by $\sigma_0\sigma(m_{K\pi\mu\mu})$,

where σ_0 is a unitless scale factor. The mean value of the B^0_d candidate mass (m_0) and σ_0 of the signal Gaussian p.d.f. are determined from fits to the control sample regions of data as described in Section 5.3. Extraction of information using the angular distribution in Equation (1) places constraints on the minimum signal yield and the signal purity in order to avoid pathological fit behaviour. A significant fraction of fits to ensembles of simulated pseudo-experiments do not converge using the full distribution. This can be mitigated using trigonometric transformations to simplify the fit as terms in Equation (1) drop out when applying these 'folding schemes'. Each transformation simplifies Equation (1) such that only three parameters are extracted from each of the four fits: F_L, S_3 and one of the other S parameters. The values and uncertainties of F_L and S_3 obtained from the four fits are consistent with each other and the results reported are those found to have the smallest systematic uncertainty. Following Ref. [3], the transformations listed below are used in order to extract the angular parameters reported here:

$$F_L, S_3, S_4, P_4^{'}: \begin{cases} \phi \rightarrow -\phi & \text{for } \phi < 0 \\ \phi \rightarrow \pi - \phi & \text{for } \theta_L > \frac{\pi}{2} \\ \theta_L \rightarrow \pi - \theta_L & \text{for } \theta_L > \frac{\pi}{2}, \end{cases} \tag{7}$$

$$F_L, S_3, S_5, P_5^{'}: \begin{cases} \phi \rightarrow -\phi & \text{for } \phi < 0 \\ \theta_L \rightarrow \pi - \theta_L & \text{for } \theta_L > \frac{\pi}{2}, \end{cases} \tag{8}$$

$$F_L, S_3, S_7, P_6^{'}: \begin{cases} \phi \rightarrow \pi - \phi & \text{for } \phi > \frac{\pi}{2} \\ \phi \rightarrow -\pi - \phi & \text{for } \phi < -\frac{\pi}{2} \\ \theta_L \rightarrow \pi - \theta_L & \text{for } \theta_L > \frac{\pi}{2}, \end{cases} \tag{9}$$

$$F_L, S_3, S_8, P_8^{'}: \begin{cases} \phi \rightarrow \pi - \phi & \text{for } \phi > \frac{\pi}{2} \\ \phi \rightarrow -\pi - \phi & \text{for } \phi < -\frac{\pi}{2} \\ \theta_L \rightarrow \pi - \theta_L & \text{for } \theta_L > \frac{\pi}{2} \\ \theta_K \rightarrow \pi - \theta_K & \text{for } \theta_L > \frac{\pi}{2}. \end{cases} \tag{10}$$

On applying transformation (7), (8), (9), and (10), the angular variable ranges become

$$\begin{aligned} \cos\theta_L \in [0,1], \cos\theta_K \in [-1,1] \text{ and } \phi \in [0,\pi], \\ \cos\theta_L \in [0,1], \cos\theta_K \in [-1,1] \text{ and } \phi \in [0,\pi], \\ \cos\theta_L \in [0,1], \cos\theta_K \in [-1,1] \text{ and } \phi \in [-\pi/2,\pi/2], \\ \cos\theta_L \in [0,1], \cos\theta_K \in [-1,1] \text{ and } \phi \in [-\pi/2,\pi/2], \end{aligned} \tag{11}$$

respectively. A consequence of using the folding schemes is that S_6 ($A_{\rm FB}$) and S_9 can not be extracted from the data. The angular parameters of interest for these schemes denoted by $\widehat{p}$ in Equation (6) are (F_L, S_3, S_i) where $i = 4, 5, 6, 8$. These translate into (F_L, P_1, P_j'), where $j = 4, 5, 7, 8$, using Equation (5).

Three MC samples are used to study signal reconstruction, acceptance, mistag and the fit performance. These assume either that the decays are flat in phase space, or follow the SM expectation taken from Ref. [24], where in the latter case separate samples are generated for B^0_d and $\overline{B}^0_d$ decays. The phase

space MC sample has $F_L = 1/3$ and the angular distributions are generated flat in $\cos\theta_K$, $\cos\theta_L$ and ϕ to study the effect of potential mistag and reconstruction differences between particle and antiparticle decays. The acceptance function is defined as the deviation from the generated distribution of $\cos\theta_K$, $\cos\theta_L$, ϕ as a result of triggering, reconstruction and selection of events. This is described by 6^{th} (2^{nd}) order polynomial distributions for $\cos\theta_K$ and $\cos\theta_L$ (ϕ) and is assumed to factorise for each angular distribution, i.e. it is assumed that $\varepsilon(\cos\theta_K, \cos\theta_L, \phi) = \varepsilon(\cos\theta_K)\varepsilon(\cos\theta_L)\varepsilon(\phi)$ is valid and a systematic uncertainty is assessed in order to account for this assumption. The acceptance function multiplies the angular distribution in the fit, i.e. neglecting the mass dependence the signal p.d.f. is

$$P_{ij} = \varepsilon(\cos\theta_K)\varepsilon(\cos\theta_L)\varepsilon(\phi)g(\cos\theta_K, \cos\theta_L, \phi), \tag{12}$$

where $g(\cos\theta_K, \cos\theta_L, \phi)$ is an angular differential decay rate resulting from one of the four folding schemes applied to Equation (1). The MC sample generated according to phase space is used to determine the nominal acceptance functions and the other samples are used for systematic uncertainty determination. The acceptance function is evaluated using the nominal sample and for each of the transformed variables defined in Equations (7-10). These functions describe the bias in the angular event distributions resulting from the reconstruction and selection. Among the angular variables the $\cos\theta_L$ distribution is the most affected by the acceptance. This is a result of the trigger thresholds and ability to reconstruct low momentum muon pairs that correspond to low values of q^2. As q^2 increases the acceptance effects become less severe. The $\cos\theta_K$ distribution is also affected by the ability to reconstruct the $K\pi$ system, however that effect shows no significant variation with q^2. There is no significant acceptance effect for ϕ. Figure 2 shows the acceptance functions used for $\cos\theta_K$ and $\cos\theta_L$ for two different q^2 ranges for the nominal angular distribution given in Equation (1).

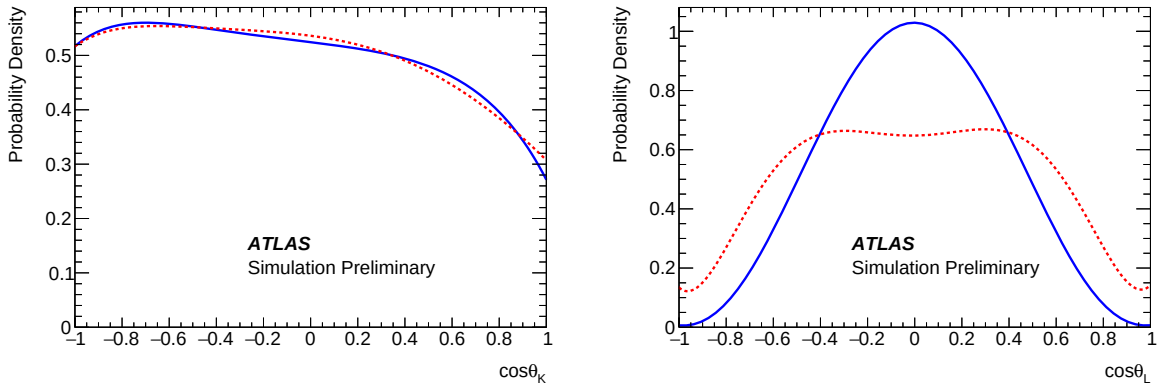

Figure 2: The acceptance functions for (left) $\cos\theta_K$ and (right) $\cos\theta_L$ for (solid) $q^2 \in [0.04, 2.0]$ GeV^2 and (dashed) $q^2 \in [4.0, 6.0]$ GeV^2 corresponding to the angular decay rate of Equation (1).

5.2 Background modes

The fit to data includes a combinatorial background component that does not peak in the $m_{K\pi\mu\mu}$ distribution. It is assumed that the background p.d.f. factorises into a product of one dimensional terms. The mass distribution of this component is described by an exponential function and second order Chebychev polynomials are used to model the $\cos\theta_K$, $\cos\theta_L$ and ϕ distributions. The nuisance parameters describing these shapes are obtained from fits to the data independently for each q^2 bin.

A total of seven inclusive and eleven exclusive B^0_d, B^0_s, B^+ and Λ_b background samples are studied in order to identify contributions of interest to be included in the fit model, or to be considered when computing systematic uncertainties. The inclusive samples considered are $b\bar{b} \to \mu^+\mu^- X$ and $c\bar{c} \to \mu^+\mu^- X$ decays and the relevant exclusive modes found to be of interest are discussed below. B_c decays are suppressed by excluding the q^2 range containing the J/ψ and $\psi(2S)$, and by charm meson vetoes discussed in Section 7. The exclusive background decays considered for the signal mode are $\Lambda_b \to \Lambda(1520)\mu^+\mu^-$, $\Lambda_b \to pK^-\mu^+\mu^-$, $B^+ \to K^{(*)+}\mu^+\mu^-$ and $B^0_s \to \phi\mu^+\mu^-$. These background contributions are accounted for as systematic uncertainties evaluated as described in Section 7.

Two distinct background contributions not considered above are observed in the $\cos\theta_K$ and $\cos\theta_L$ distributions. They are not accounted for in the nominal fit to data, and are treated as systematic effects. The peak in $\cos\theta_K$ is found to be around 1.0 and appears to have two types of contribution. One of these arises from mis-reconstructed B^+ decays, such as $B^+ \to K^+\mu\mu$ and $B^+ \to \pi^+\mu\mu$. These decays can be reconstructed as signal if another track is combined with the hadron to form a K^* candidate in such a way that the event passes the reconstruction and selection. Events with a three track invariant mass, formed from one of the hadrons from the K^* candidate and the two muon candidates, that fall within a 50 MeV mass window relative to the nominal B^+ mass are removed from data when studying systematic uncertainties. This veto reduces the amount of data accumulated in $\cos\theta_K$ around 1.0 and has a small effect on the signal efficiency. The second contribution comes from combinations of two charged tracks that pass the selection and are reconstructed as a K^* candidate. These fake K^* candidates accumulate around $\cos\theta_K$ of 1.0 and are observed in the $K\pi$ sidebands away from the K^* meson. They are distinct from the resonant structure of expected S, P and D-wave $K\pi$ decays resulting from a $B^0_d \to K\pi\mu\mu$ transition. The origin of this source of background is not fully understood. The observed excess may arise from a statistical fluctuation, an unknown background process, or a combination of both. All events are retained for the nominal fit this region ($\cos\theta_K > 0.9$) is removed when evaluating systematic uncertainties.

The background that peaks in $\cos\theta_L$ is studied using Monte Carlo simulated events for the decays $D^0 \to K\pi$, $D^+ \to K\pi\pi$, $D^+_s \to KK\pi$, and $D^{*+}_s \to KK\pi$. Events with an intermediate charm meson, D^0, $D^\pm_{(s)}$ and D^{*+}_s are found to pass the selection and are reconstructed in such a way that they accumulate around 0.7 in $|\cos\theta_L|$. These are removed from the data sample when studying systematic uncertainties by applying a veto window about the reconstructed charm meson mass. The optimal veto window is found to be 30 MeV wide using MC simulated events. A few percent of signal events are lost using these vetoes and a narrow hole in the $\cos\theta_L$ acceptance distribution is created near $|\cos\theta_L|$ of 0.7.

5.3 $K^*c\bar{c}$ control sample fits

The mass distribution obtained in MC simulated samples for $K^*c\bar{c}$ decays and the signal, in different bins of q^2, are found to be consistent with each other. Fits to the data are used to extract values of m_0 and σ_0 for $B^0_d \to K^*J/\psi$ and $B^0_d \to K^*\psi(2S)$ events that are used for the signal p.d.f. An extended unbinned maximum likelihood fit is performed to the two $K^*c\bar{c}$ control sample regions allowing for 0, 1, 2 and 3 exclusive background components. The exclusive backgrounds included are $\Lambda_b \to \Lambda c\bar{c}$, $B^+ \to K^+c\bar{c}$ and $B_s \to K^*c\bar{c}$, respectively. The $K^*c\bar{c}$ p.d.f. has the same form as the signal model, combinatorial background is described by an exponential distribution, and double and triple Gaussian p.d.f.s determined from MC simulated events are used to describe the exclusive background contributions. The resulting distributions for the three exclusive background fits can be found in Figure 3. The peak position and scale factor of the signal p.d.f. are not sensitive to the exclusive background model used. From these fits the statistical and systematic uncertainties on the values of m_0 and σ_0 are extracted for the B^0_d component in

order to be used when the $B_d^0 \to K^*\mu^+\mu^-$ fits are performed. From the J/ψ control data it is determined that the signal $K\pi\mu\mu$ mass p.d.f. model nuisance parameters are $m_0 = (5276.6 \pm 0.3 \pm 0.4)$ MeV and $\sigma_0 = 1.210 \pm 0.004 \pm 0.002$, where the uncertainties are statistical and systematic, respectively. The $\psi(2S)$ sample yields compatible results albeit with larger uncertainties. These results are similar to those obtained from the MC simulated samples, and the numbers derived from the K^*J/ψ data are used for the signal region fits.

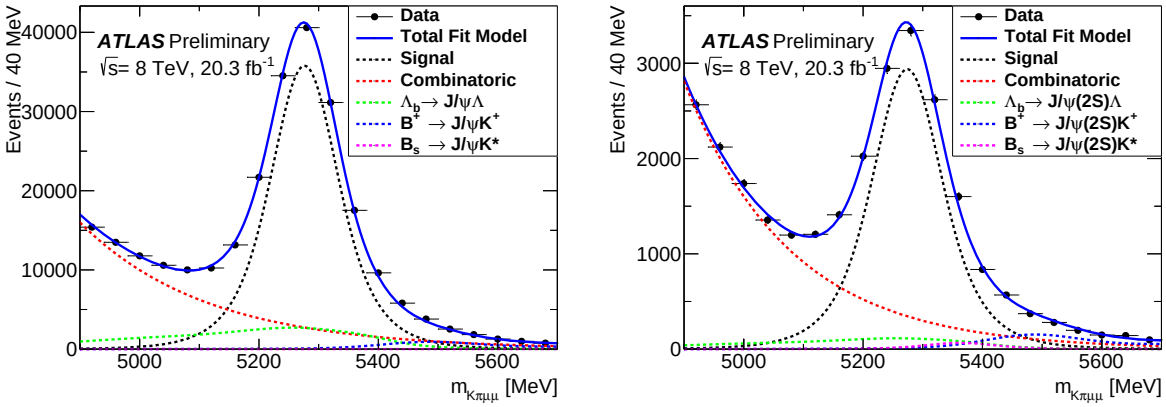

Figure 3: Control sample fits to the $K\pi\mu\mu$ invariant mass distributions for the (left) K^*J/ψ and (right) $K^*\psi(2S)$ regions. The data are shown as points and the total fit model as the solid lines. The dashed lines represent (black) signal, (red) combinatorial background, (green) Λ_b background, (blue) B^+ background and (magenta) B_s^0 background.

5.4 Fitting procedure and validation

A two-step fit process is performed for the different signal regions in q^2. The first step is a fit to the $K\pi\mu^+\mu^-$ invariant mass distribution, using the event-by-event uncertainty on the reconstructed mass as a conditional variable. For this fit the parameters m_0 and σ_0 are fixed to the values obtained from fits to data control samples as described in Section 5.3. A second step adds the (transformed) $\cos\theta_K$, $\cos\theta_L$ and ϕ variables to the likelihood in order to extract F_L and the S_i parameters along with nuisance parameters related to the combinatorial background shapes. The nuisance parameters (m_0, σ_0, signal and background yields, and the exponential shape parameter for the background mass p.d.f.) are fixed to the nominal results obtained from the first step.

The fit procedure is validated using ensembles of simulated pseudo-experiments generated with the F_L and S parameters corresponding to those obtained from the data. The purpose of these experiments is to measure the intrinsic fit bias resulting from the likelihood estimator used to extract signal parameters. These ensembles are also used to validate that the uncertainty extracted from the fit is consistent with expectations. Ensembles of simulated pseudo-experiments are performed where signal MC is injected into samples of background events generated from the likelihood. The signal yield determined from the first step in the fit process is found to be unbiased. The angular parameters extracted from the nominal fits have biases ranging between 0.01 and 0.04, depending on the fit variation and q^2 bin. A similar procedure is used to estimate the effect of neglecting S-wave contamination in the data sample. Neglecting the S-wave component in the fit model results in a bias of between between 0.00 and 0.02 on the angular parameters.

Similarly neglecting exclusive background contributions from Λ_b, B^+ and B_s^0 decays that peak in $m_{K\pi\mu\mu}$ corresponds to a bias of less than 0.01 on the angular parameters. The $P_i^{(\prime)}$ parameters are obtained using the fit results and covariance matrices from the second fit along with Equations (2–5).

6 Results

Event yields obtained from the fits are summarised in Table 1 where only statistical uncertainties are reported. Figures 4 through 9 show distributions of the variables used in the fit for the S_5 folding scheme (corresponding to the transformation of Equation (8)) with the total, signal and background fitted p.d.f.s superimposed. Similar sets of distributions are obtained for the three other folding schemes: S_4, S_7 and S_8. The results of the angular fits to the data in terms of the S_i and $P_i^{(\prime)}$ can be found in Tables 2 and 3. Statistical and systematic uncertainties are quoted in the tables. The distributions of F_L and the S parameters as a function of q^2 are shown in Figure 10 and those for $P_i^{(\prime)}$ are shown in Figure 11.

Table 1: The values of fitted signal, n_{signal}, and background, $n_{\text{background}}$, yields obtained for different bins in q^2. The uncertainties indicated are statistical.

q^2 [GeV^2]	n_{signal}	$n_{\text{background}}$
[0.04, 2.0]	128 ± 22	122 ± 22
[2.0, 4.0]	106 ± 23	113 ± 23
[4.0, 6.0]	114 ± 24	204 ± 26
[0.04, 4.0]	236 ± 31	233 ± 32
[1.1, 6.0]	275 ± 35	363 ± 36
[0.04, 6.0]	342 ± 39	445 ± 40

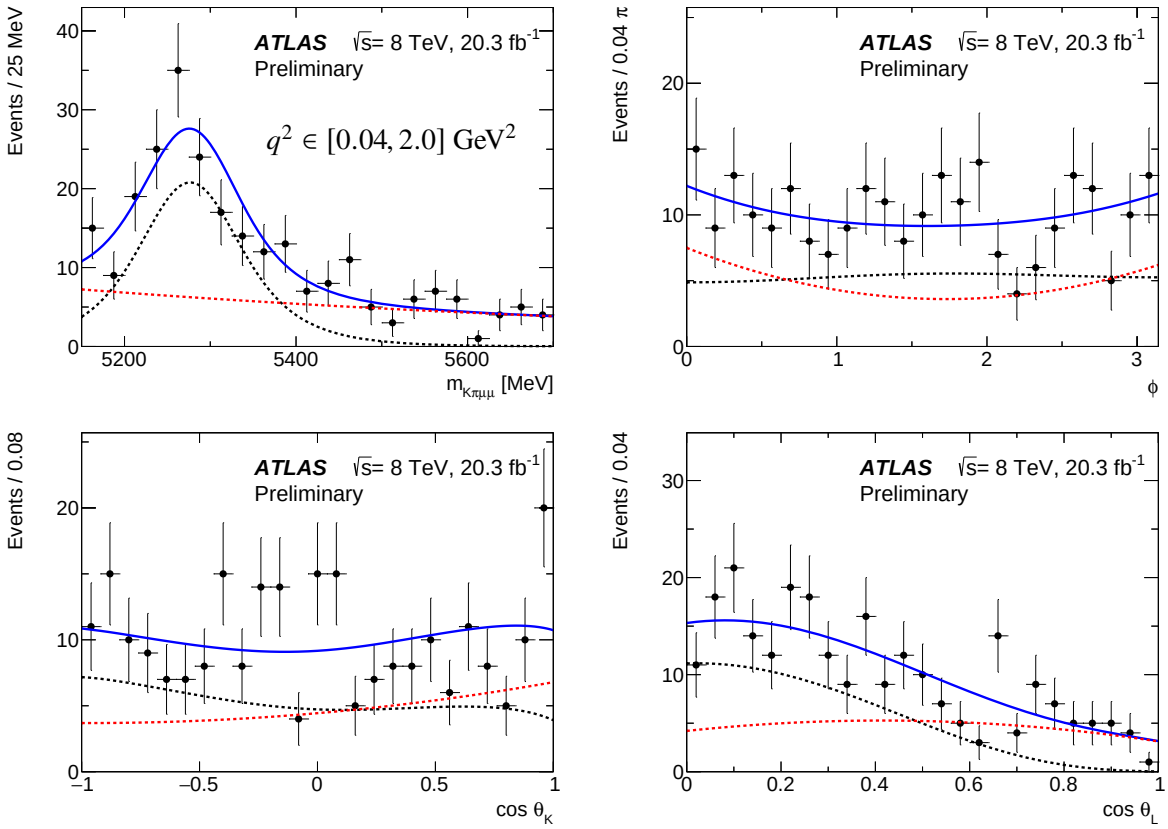

Figure 4: The distributions of (top left) $m_{K\pi\mu\mu}$, (top right) ϕ, (bottom left) $\cos\theta_K$, and (bottom right) $\cos\theta_L$ obtained for $q^2 \in [0.04, 2.0]$ GeV^2. The (blue) solid line is a projection of the total p.d.f., the (red) dashed line represents the background, and the (black) dashed line represents the signal component. These plots are obtained from a fit using the S_5 folding scheme.

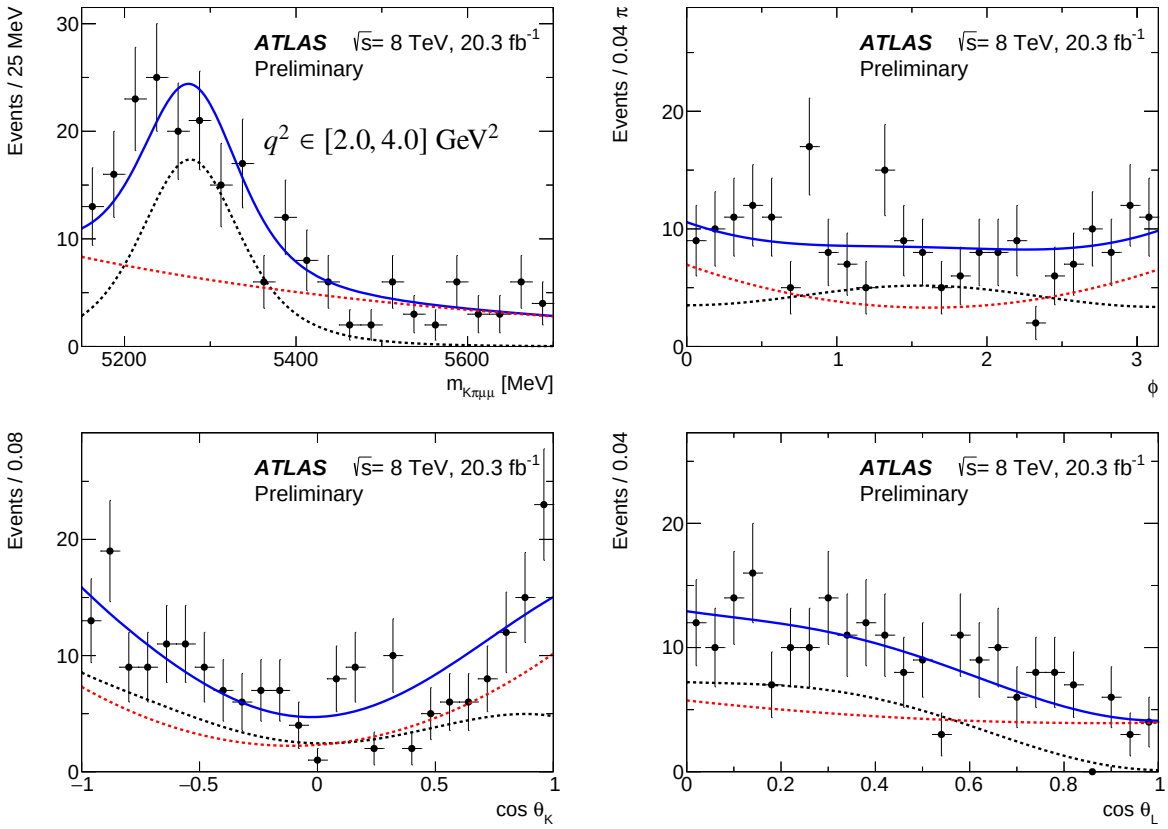

Figure 5: The distributions of (top left) $m_{K\pi\mu\mu}$, (top right) ϕ, (bottom left) $\cos\theta_K$, and (bottom right) $\cos\theta_L$ obtained for $q^2 \in [2.0, 4.0]$ GeV^2. The (blue) solid line is a projection of the total p.d.f., the (red) dashed line represents the background, and the (black) dashed line represents the signal component. These plots are obtained from a fit using the S_5 folding scheme.

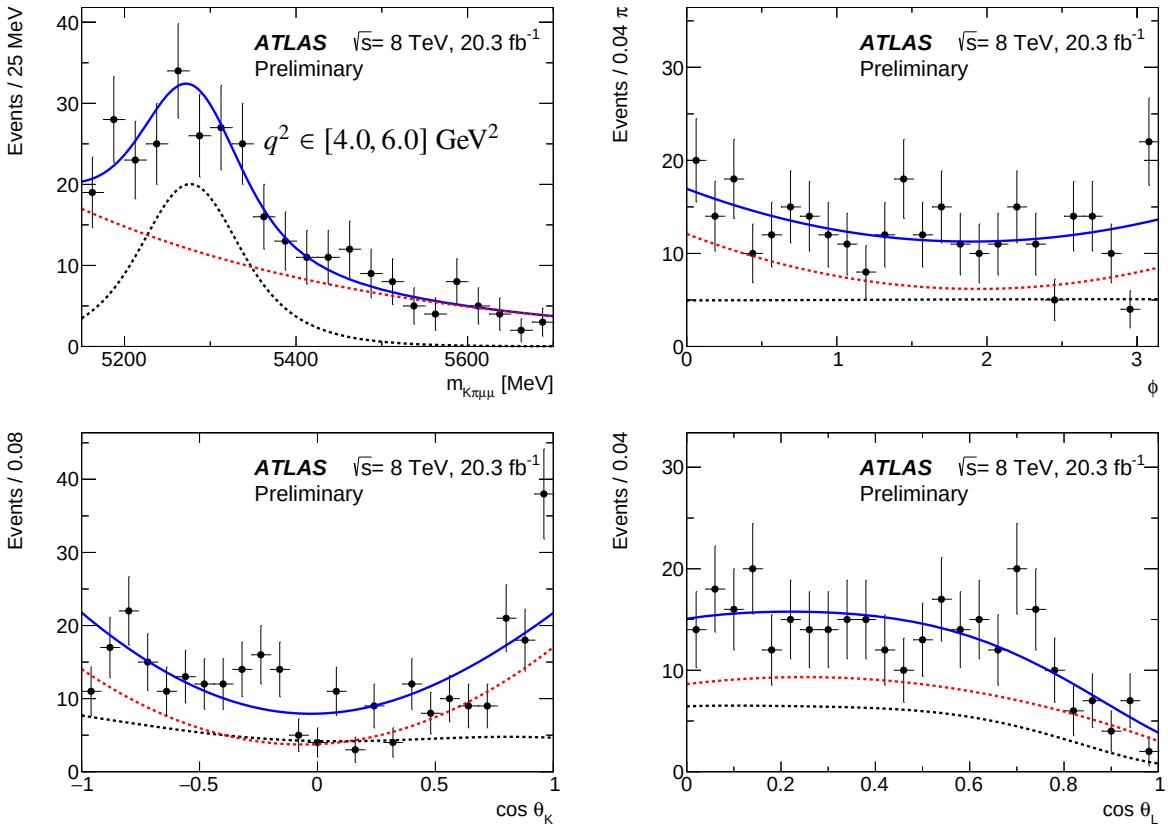

Figure 6: The distributions of (top left) $m_{K\pi\mu\mu}$, (top right) ϕ, (bottom left) $\cos\theta_K$, and (bottom right) $\cos\theta_L$ obtained for $q^2 \in [4.0, 6.0]$ GeV^2. The (blue) solid line is a projection of the total p.d.f., the (red) dashed line represents the background, and the (black) dashed line represents the signal component. These plots are obtained from a fit using the S_5 folding scheme.

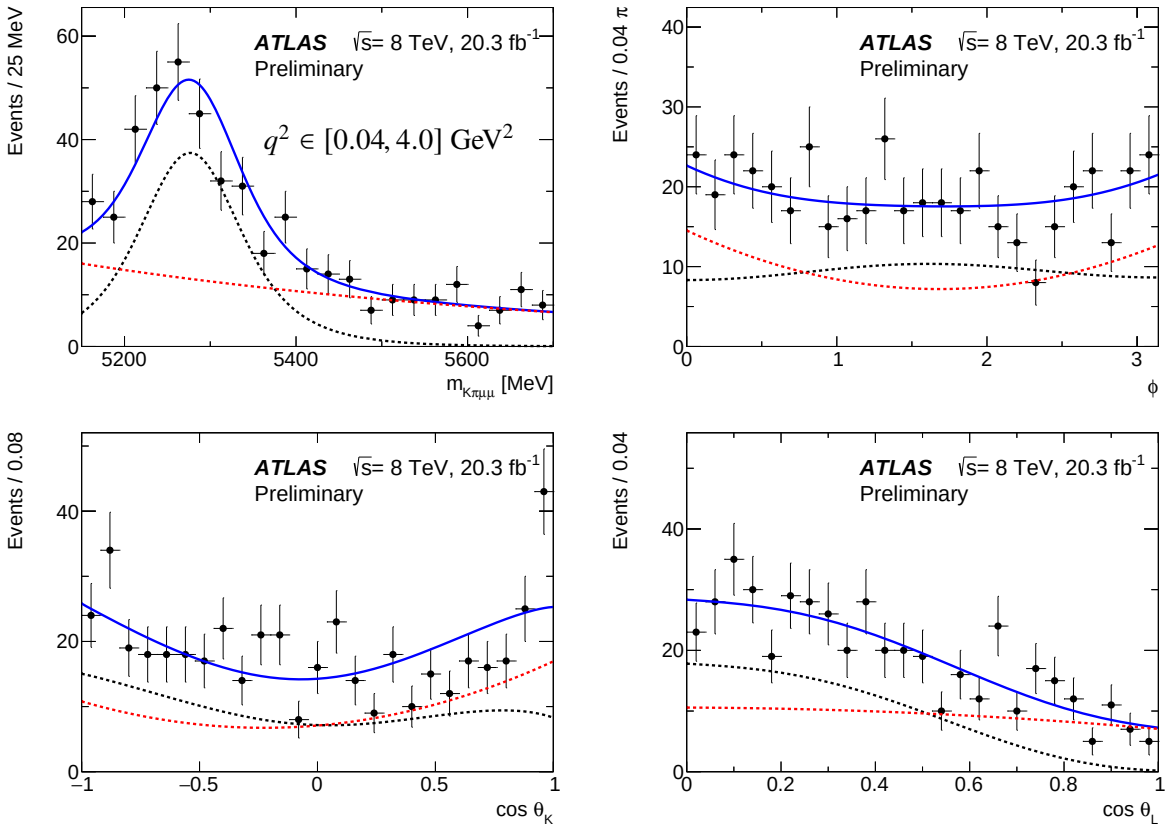

Figure 7: The distributions of (top left) $m_{K\pi\mu\mu}$, (top right) ϕ, (bottom left) $\cos\theta_K$, and (bottom right) $\cos\theta_L$ obtained for $q^2 \in [0.04, 4.0]$ GeV^2. The (blue) solid line is a projection of the total p.d.f., the (red) dashed line represents the background, and the (black) dashed line represents the signal component. These plots are obtained from a fit using the S_5 folding scheme.

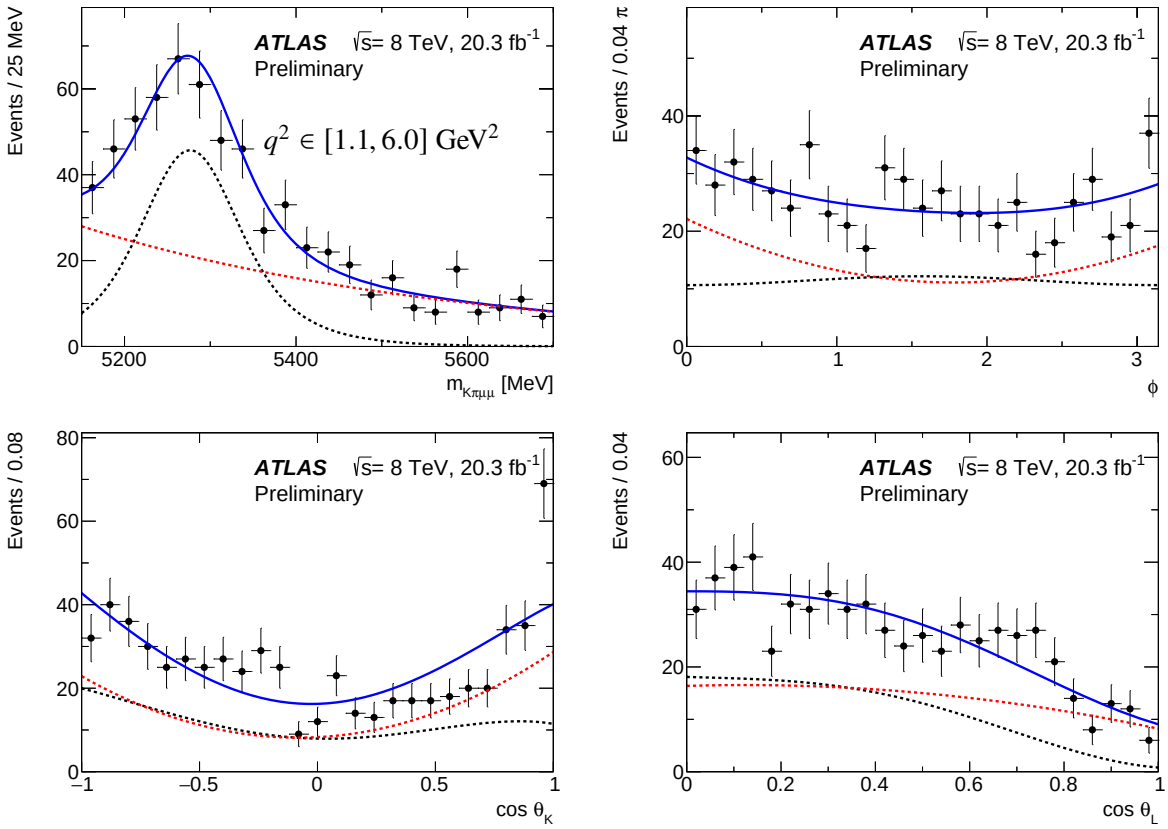

Figure 8: The distributions of (top left) $m_{K\pi\mu\mu}$, (top right) ϕ, (bottom left) $\cos\theta_K$, and (bottom right) $\cos\theta_L$ obtained for $q^2 \in [1.1, 6.0]$ GeV^2. The (blue) solid line is a projection of the total p.d.f., the (red) dashed line represents the background, and the (black) dashed line represents the signal component. These plots are obtained from a fit using the S_5 folding scheme.

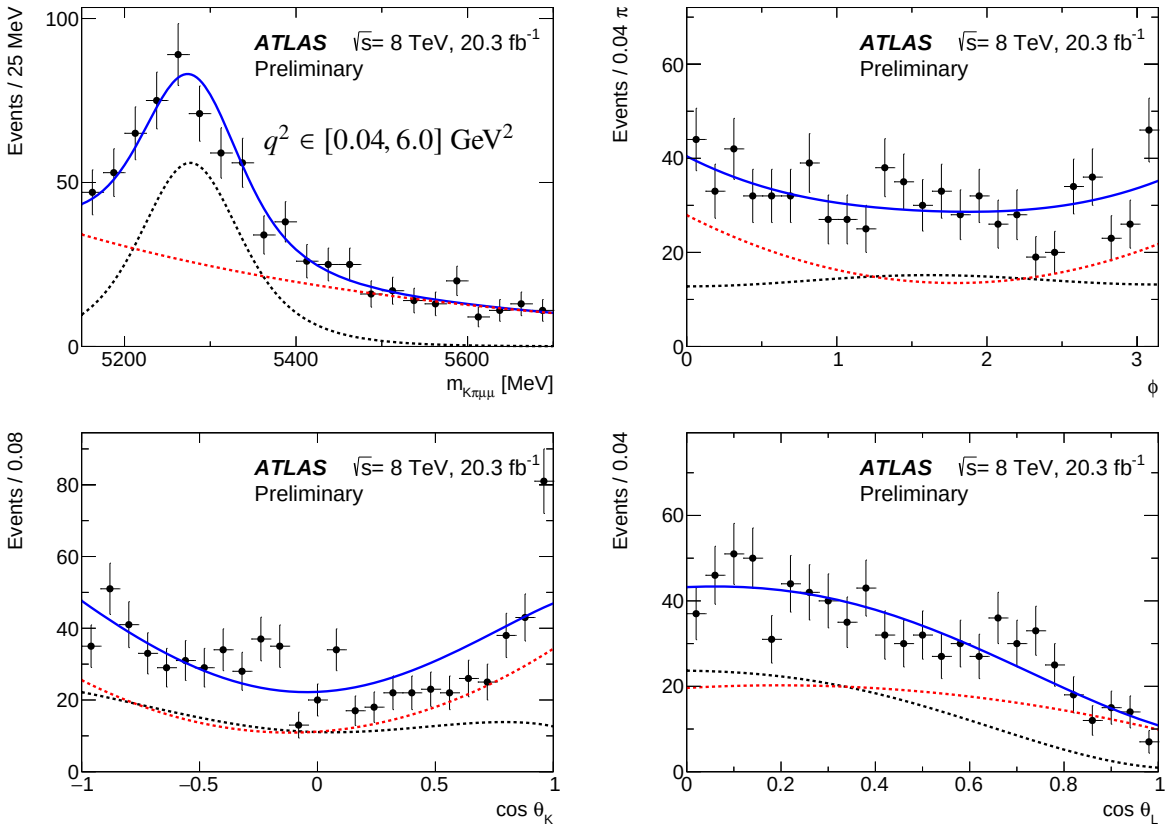

Figure 9: The distributions of (top left) $m_{K\pi\mu\mu}$, (top right) ϕ, (bottom left) $\cos\theta_K$, and (bottom right) $\cos\theta_L$ obtained for $q^2 \in [0.04, 6.0]$ GeV^2. The (blue) solid line is a projection of the total p.d.f., the (red) dashed line represents the background, and the (black) dashed line represents the signal component. These plots are obtained from a fit using the S_5 folding scheme.

Table 2: The values F_L, and S_3, S_4, S_5, S_7 and S_8 obtained for different bins in q^2. The uncertainties indicated are statistical and systematic, respectively.

q^2 [GeV^2]	F_L	S_3	S_4	S_5	S_7	S_8
[0.04, 2.0]	$0.44 \pm 0.08 \pm 0.07$	$-0.02 \pm 0.09 \pm 0.02$	$0.19 \pm 0.25 \pm 0.10$	$0.33 \pm 0.13 \pm 0.06$	$-0.09 \pm 0.10 \pm 0.02$	$-0.11 \pm 0.19 \pm 0.07$
[2.0, 4.0]	$0.64 \pm 0.11 \pm 0.05$	$-0.15 \pm 0.10 \pm 0.07$	$-0.47 \pm 0.19 \pm 0.10$	$-0.16 \pm 0.15 \pm 0.05$	$0.15 \pm 0.14 \pm 0.09$	$0.41 \pm 0.16 \pm 0.15$
[4.0, 6.0]	$0.42 \pm 0.13 \pm 0.12$	$0.00 \pm 0.12 \pm 0.07$	$0.40 \pm 0.21 \pm 0.09$	$0.13 \pm 0.18 \pm 0.07$	$0.03 \pm 0.13 \pm 0.07$	$-0.09 \pm 0.16 \pm 0.04$
[0.04, 4.0]	$0.52 \pm 0.07 \pm 0.06$	$-0.05 \pm 0.06 \pm 0.04$	$-0.19 \pm 0.16 \pm 0.09$	$0.16 \pm 0.10 \pm 0.04$	$0.01 \pm 0.08 \pm 0.05$	$0.15 \pm 0.13 \pm 0.10$
[1.1, 6.0]	$0.56 \pm 0.07 \pm 0.06$	$-0.04 \pm 0.07 \pm 0.03$	$0.03 \pm 0.14 \pm 0.07$	$0.00 \pm 0.10 \pm 0.03$	$0.02 \pm 0.08 \pm 0.06$	$0.09 \pm 0.11 \pm 0.08$
[0.04, 6.0]	$0.50 \pm 0.06 \pm 0.04$	$-0.04 \pm 0.06 \pm 0.03$	$0.03 \pm 0.13 \pm 0.07$	$0.14 \pm 0.09 \pm 0.03$	$0.02 \pm 0.07 \pm 0.05$	$0.05 \pm 0.10 \pm 0.07$

Table 3: The values P_1, P_4', P_5', P_6' and P_8' obtained for different bins in q^2. The uncertainties indicated are statistical and systematic, respectively.

q^2 [GeV^2]	P_1	P_4'	P_5'	P_6'	P_8'
[0.04, 2.0]	$-0.06 \pm 0.30 \pm 0.10$	$0.39 \pm 0.51 \pm 0.25$	$0.67 \pm 0.26 \pm 0.16$	$-0.18 \pm 0.21 \pm 0.04$	$-0.22 \pm 0.38 \pm 0.14$
[2.0, 4.0]	$-0.78 \pm 0.51 \pm 0.42$	$-0.96 \pm 0.39 \pm 0.26$	$-0.33 \pm 0.31 \pm 0.13$	$0.31 \pm 0.28 \pm 0.19$	$0.84 \pm 0.32 \pm 0.31$
[4.0, 6.0]	$0.00 \pm 0.47 \pm 0.26$	$0.81 \pm 0.42 \pm 0.24$	$0.26 \pm 0.35 \pm 0.17$	$0.06 \pm 0.27 \pm 0.13$	$-0.19 \pm 0.33 \pm 0.07$
[0.04, 4.0]	$-0.22 \pm 0.26 \pm 0.16$	$-0.38 \pm 0.31 \pm 0.22$	$0.32 \pm 0.21 \pm 0.10$	$0.01 \pm 0.17 \pm 0.10$	$0.30 \pm 0.26 \pm 0.19$
[1.1, 6.0]	$-0.17 \pm 0.31 \pm 0.14$	$0.07 \pm 0.28 \pm 0.18$	$0.01 \pm 0.21 \pm 0.07$	$0.03 \pm 0.17 \pm 0.11$	$0.18 \pm 0.22 \pm 0.16$
[0.04, 6.0]	$-0.15 \pm 0.23 \pm 0.10$	$0.07 \pm 0.26 \pm 0.18$	$0.27 \pm 0.19 \pm 0.07$	$0.03 \pm 0.15 \pm 0.10$	$0.11 \pm 0.21 \pm 0.14$

7 Systematic uncertainties

A number of sources of systematic uncertainty on the parameters obtained from the angular analysis are considered. The methods for determining these are based on either a comparison of nominal and modified fit results, or on observed fit biases in modified pseudo-experiments. The systematic uncertainties are symmetrised. The most significant ones are described in the following, in order of importance.

- A systematic uncertainty is assigned for the combinatorial $K\pi$ (fake K^*) background peaking at $\cos\theta_K$ values around 1.0 obtained by comparing results of the nominal fit to that where data above $\cos\theta_K = 0.9$ are excluded from the result.
- A systematic uncertainty is derived to account for background arising from partially reconstructed $B \to D^0/D^+/D_s^+/D_s^*X$ decays, that manifest in an accumulation of events at $|\cos\theta_L|$ values around 0.7. Two or three track combinations are formed from the signal candidate tracks, and are reconstructed assuming the pion or kaon mass hypothesis. A veto is then applied for events in which a track combination has a mass in a window of 30 MeV around the $D_{(s)}^{(*)}$ meson mass. Similarly a veto is implemented to reject $B^+ \to K^+\mu^+\mu^-$ and $B^+ \to \pi^+\mu^+\mu^-$ events that pass the event selection. Here B^+ candidates are reconstructed from one of the hadrons from the K^* candidate and the muons in the signal candidate. Signal candidates that have the three track mass within 50 MeV of the B^+ mass are assumed to be from a B^+ decay and are excluded from the fit. A few percent of signal events are removed on applying these vetoes. The fit results obtained from the data samples with vetoes applied are compared to those obtained from the nominal fit and the change in result is taken as the systematic uncertainty from these backgrounds. This systematic uncertainty dominates the measurement of F_L at higher values of q^2.
- The background p.d.f. shape has an uncertainty arising from the choice of the model. For the mass distribution it is assumed that an exponential decay model is adequate, however for the angular variables the data are re-fitted using third order Chebychev polynomials. The change in result from nominal is taken as the uncertainty from this source.
- The acceptance function is assumed to factorise into three separate components, one each for $\cos\theta_K$, $\cos\theta_L$ and ϕ. To validate this assumption the signal MC data is fitted with the acceptance function obtained from that sample. Differences from expectation are small and taken as the uncertainty resulting from this assumption.
- Combinatorial background is the dominant source of background. An uncertainty on the modeling and normalisation of this component is computed by comparing the nominal result to that with a reduced fit range of $m_{K\pi\mu\mu} \in [5200, 5700]$ MeV.
- A correction is applied to the data by smearing the track $p_{\rm T}$ according to the uncertainties arising from biases in rapidity and momentum scale. The change in results obtained is ascribed to the uncertainty in the ID alignment and knowledge of the magnetic field.
- The maximum likelihood estimator used is intrinsically biased. Ensembles of MC simulated events are used in order to ascertain the bias on the extracted parameters of interest. The bias is assigned as a systematic uncertainty.
- The $p_{\rm T}$ spectrum of B candidates observed in data is not accurately reproduced by the MC simulation. The effect of this difference on the kinematics of signal decays, changes the acceptance functions. This is accounted for by reweighting signal MC simulated events to resemble the $p_{\rm T}$ spectrum found

in data. The change in fitted parameters obtained due to the reweighting is taken as the systematic uncertainty resulting from this difference. The weights used are determined from background subtracted $B^0_d \to K^* J/\psi$ control region data.

- The signal decay mode proceeds via a resonant $K^* \to K\pi$ decay. Scalar contributions from non-resonant $K\pi$ transitions may exist. The LHCb Collaboration have reported an S-wave contribution at the level of 5% of the signal [4, 25]. Ensembles of MC simulated events are fitted with 5% of the signal being drawn from an S-wave sample of events and the remaining 95% from signal. The observed change in fit bias is assigned as the systematic uncertainty from this source. Any variation in S-wave content as a function of q^2 would not significantly affect the results reported here.

- Nuisance parameters from the fit model obtained from MC control samples and mass fits to the data have associated uncertainties. These parameters include m_0, σ_0, the signal and background yields, the shape parameter of the combinatoric background mass distribution, and the parameters of the signal acceptance functions. The uncertainty on each of these parameters is varied independently in order to assess the effect on parameters of interest. This source of uncertainty is a small contribution the measurements reported here.

- Background from exclusive modes peaking in $m_{K\pi\mu\mu}$ is neglected in the nominal fit. This may affect the fitted results and is accounted for by computing the fit bias obtained when embedding MC simulated samples of $\Lambda_b \to \Lambda(1520)\mu^+\mu^-$, $\Lambda_b \to pK^-\mu^+\mu^-$, $B^+ \to K^{(*)+}\mu^+\mu^-$ and $B^0_s \to \phi\mu^+\mu^-$ into ensembles of pseudo-data generated starting from the fit model containing only combinatorial background and signal components. The change in fit bias observed on adding exclusive backgrounds is taken as the systematic error arising from neglecting those modes in the fit.

- The difference from nominal results obtained when fitting the B^0_d signal MC with the acceptance function for $\overline{B}^0_d$ is taken as the systematic error resulting from event migration due to misreconstructing the signal.

- S_4 and S_5, as well as the respective $P_i^{(\prime)}$ parameters are affected by dilution and thus have a multiplicative scaling applied to them. The effect of data/MC differences in the $p_{\rm T}$ spectrum of B candidates on the mistag probability has been studied and found to be negligible. The uncertainty due to the number of MC events is used to compute the uncertainty on ω and $\overline{\omega}$. Studies of MC simulated events indicate that there is no significant difference between the mistag probability for B^0_d and $\overline{B}^0_d$ events and the analysis assumes an average mistag probability provides an adequate description of this effect. The magnitude of the mistag probability difference, $|\omega - \overline{\omega}|$, is included as a systematic uncertainty resulting from this assumption.

The total systematic uncertainties for the S_i and $P_i^{(\prime)}$ parameters fitted are presented in Tables 2 and 3, where the dominant contributions for F_L come from the background angular variable modeling and the partially reconstructed decays peaking in $\cos\theta_K$ and $\cos\theta_L$. These contributions also affect S_3 (P_1) as does the ID alignment and B field calibration. The largest systematic uncertainty contribution to S_3 (P_1) comes from partially reconstructed decays feeding up into the signal region. This also affects the measurement of S_5 (P'_5) and S_7 (P'_6). The partially reconstructed decays peaking in $\cos\theta_L$ affect the measurement of S_4 (P'_4) and S_8 (P'_8), whereas the fake K^* background in $\cos\theta_K$ affects S_4 (P'_4), S_5 (P'_5), and S_8 (P'_8). The parameterisation of the signal acceptance is another significant systematic uncertainty source for S_4 (P'_4). The systematic uncertainties are smaller than the statistical uncertainties for all parameters measured.

8 Comparison with theoretical computations

The results of theoretical approaches of Ciuchini et al. (CFFMPSV) [26], Descotes-Genon et al. (DHMV) [27], and Jäger and Camalich (JC) [28, 29] are shown in Figure 10 for the S parameters, and in Figure 11 for the $P^{(\prime)}$ parameters, along with the results presented here[4].

QCD factorisation is used by DHMV and JC, where the latter focus on the impact of long distance corrections using a helicity amplitude approach. The CFFMPSV group takes a different approach, using the QCD factorisation framework to perform consistency checks of the LHCb data with theory expectations. This approach also allows information from a given experimentally measured parameter of interest to be excluded in order to make a fit-based prediction of the expected value of that parameter from the rest of the data.

With the exception of the P_4' and P_5' measurements in $q^2 \in [4.0, 6.0]$ GeV^2 and P_8' in $q^2 \in [2.0, 4.0]$ GeV^2 there is good agreement between theory and measurement. The deviation, relative to SM calculations, observed for P_4' (P_5') is consistent with the deviation reported by the LHCb Collaboration in Ref. [4], and it is approximately 2.5 (2.7) standard deviations away from the calculation of DHMV. The deviations are less significant for the other calculation and the fit approach. All measurements are found to be within three standard deviations of the range covered by the different predictions. Hence, including experimental and theoretical uncertainties, the measurements presented here are found to be in accordance with the expectations of the SM contributions to this decay.

[4] This result uses the experimental convention of Equations (2)-(5) following the LHCb Collaboration's notation of Ref. [3]. The theory community uses different conventions: DHMV use the convention explained by Equation (16) of Ref. [12].

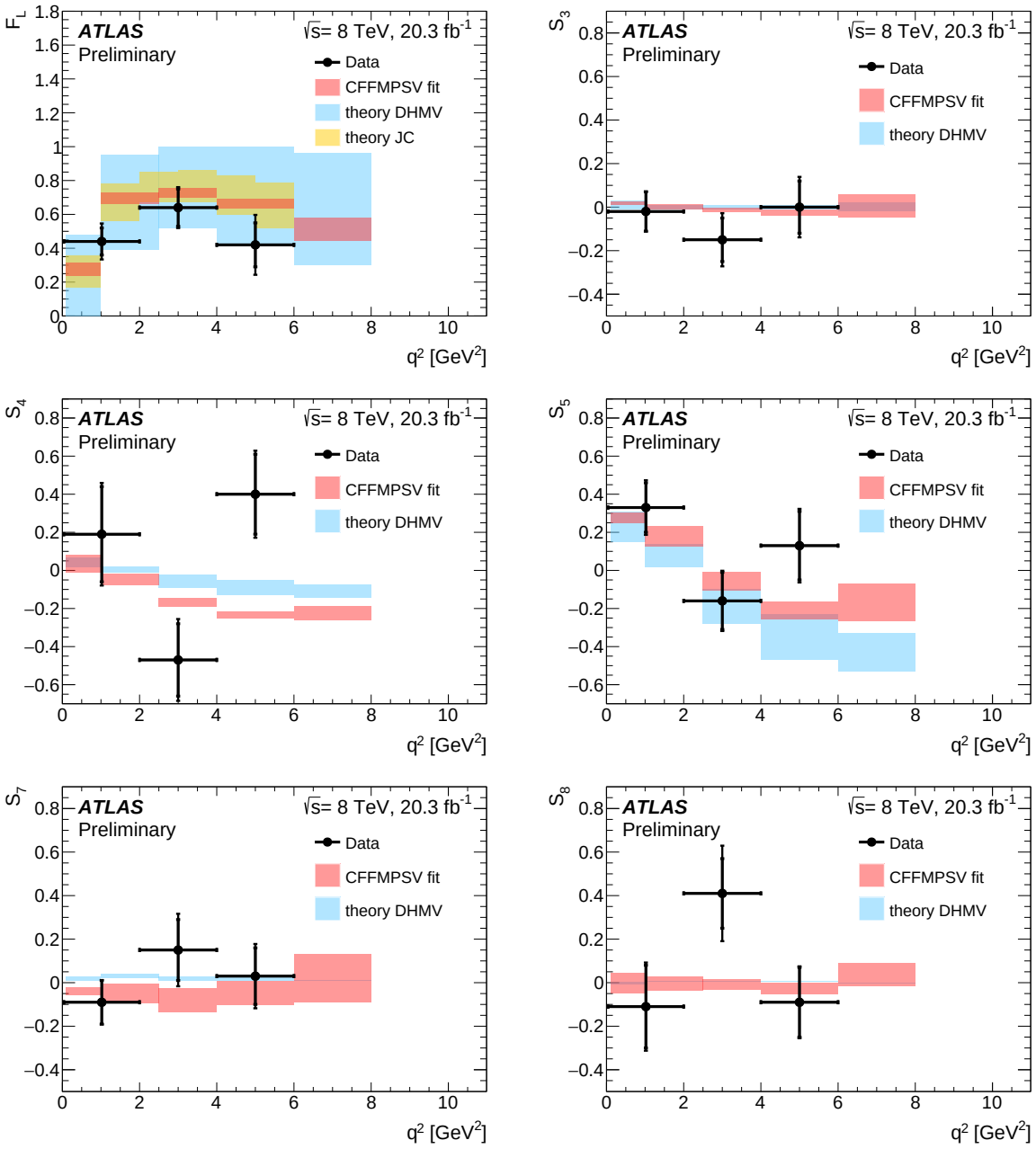

Figure 10: The measured values of F_L, S_3, S_4, S_5, S_7, S_8 compared with predictions from the theoretical calculations discussed in the text (Section 8). Statistical and total uncertainties are shown for the data, i.e. the inner mark indicates the statistical uncertainty and the total error bar the total uncertainty.

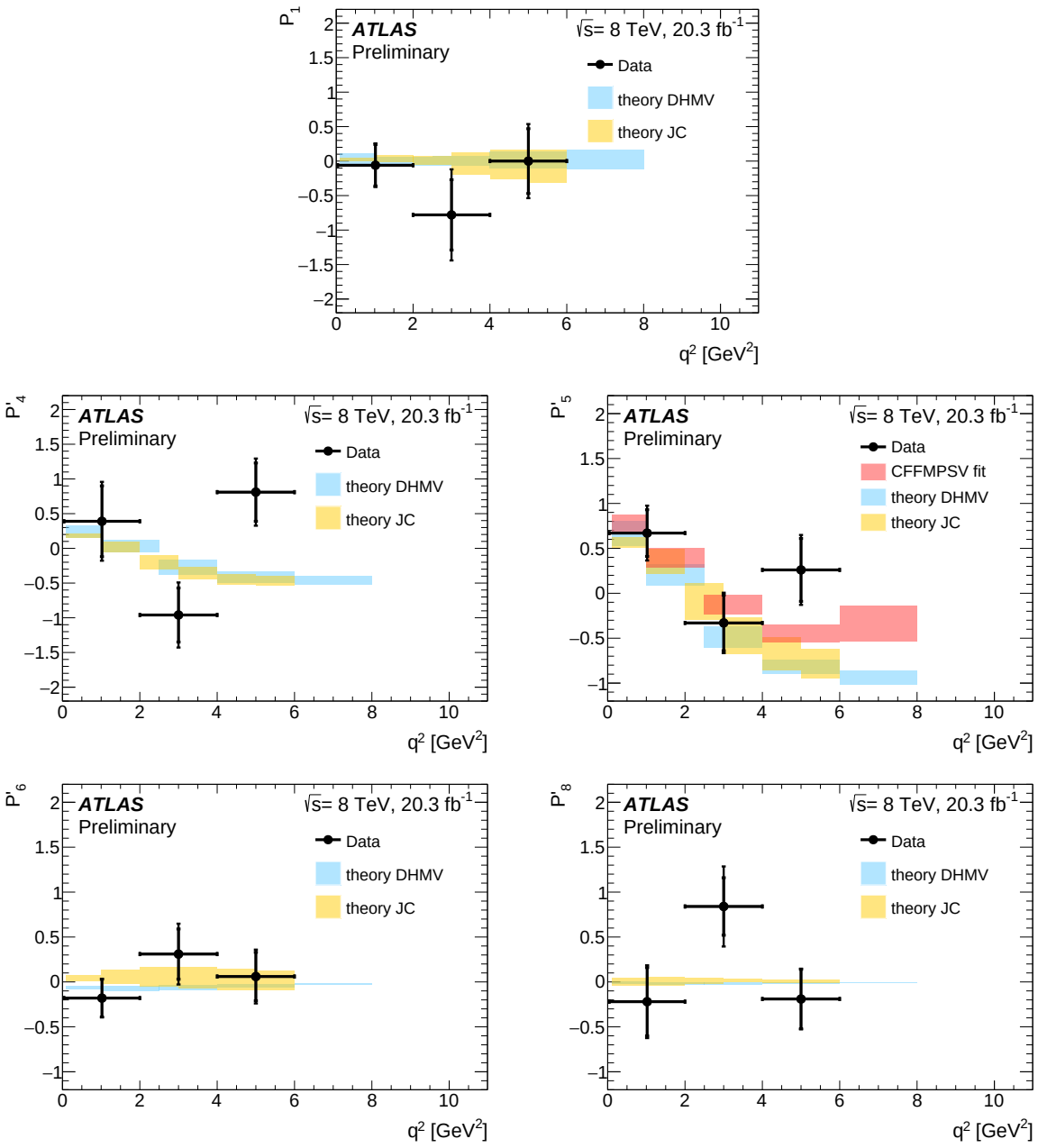

Figure 11: The measured values of P_1, P_4', P_5', P_6', P_8' compared with predictions from the theoretical calculations discussed in the text (Section 8). Statistical and total uncertainties are shown for the data, i.e. the inner mark indicates the statistical uncertainty and the total error bar the total uncertainty.

9 Conclusion

The results of an angular analysis of the rare decay $B_d^0 \to K^*\mu^+\mu^-$ have been presented. This flavor changing neutral current process is sensitive to potential new physics contributions. The $B_d^0 \to K^*\mu^+\mu^-$ analysis presented here uses a total of 20.3 fb^{-1} of $\sqrt{s} = 8$ TeV pp collision data collected by the ATLAS experiment at the LHC in 2012. An extended unbinned maximum likelihood fit of the angular distribution of the signal decay is performed in order to extract the parameters F_L, S_i and $P_i^{(\prime)}$ in six bins of q^2. Three of these bins are overlapping in order to report results in ranges compatible with other experiments and phenomenology studies. All measurements are found to be within three standard deviation of the range covered by the different predictions. The results are also compatible with the results of the LHCb and Belle Collaborations.

Appendix

The leading order SM processes for the decay $B^0_d \to K^* \mu^+ \mu^-$ are shown in Figure 12.

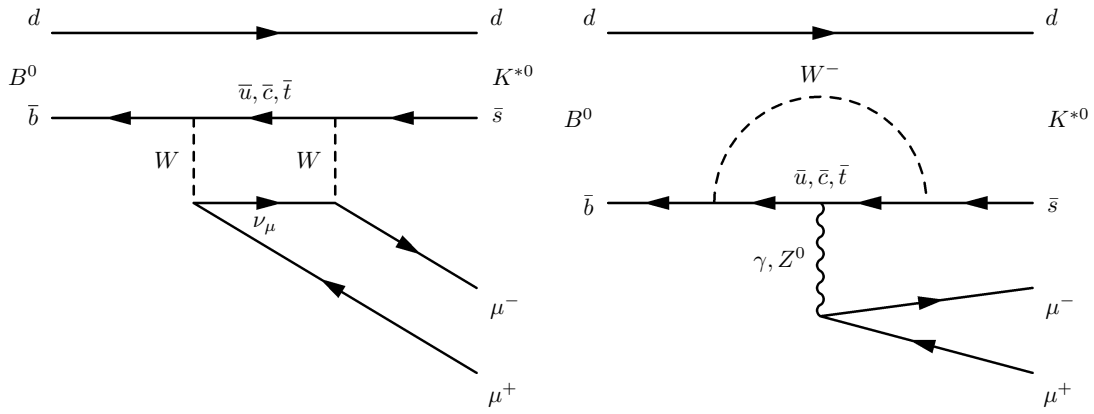

Figure 12: Box and penguin diagrams of $B^0_d \to K^* \mu^+ \mu^-$ decay.

The results presented in Section 8 are compared with theoretical calculations and phenomenological fit results. The only results displayed in that Section are from the ATLAS Collaboration. These results are presented here along with those from the *BABAR*, Belle, CMS and LHCb Collaborations. Figures 13 and 14 show the results obtained as a function of q^2 for the S_i and F_L parameters, and for the $P_i^{(\prime)}$, respectively. The ensemble of experimental results are also presented without any theory calculation or phenomenological fit overlaid in Figures 15 and 16.

Section 7 details the various systematic uncertainty sources considered for this analysis and Tables 2 and 3 show the total systematic uncertainty computed for F_L and the S_i. The uncertainties for S_i are translated to the $P_i^{(\prime)}$ equivalents using Equations (2) through (5). The relative contributions of the different systematic effects on the total systematic uncertainty for F_L and the S_i are indicated in Table 4. This table lists either the largest or range of systematic uncertainty contributing to the measurement of one of the angular parameters.

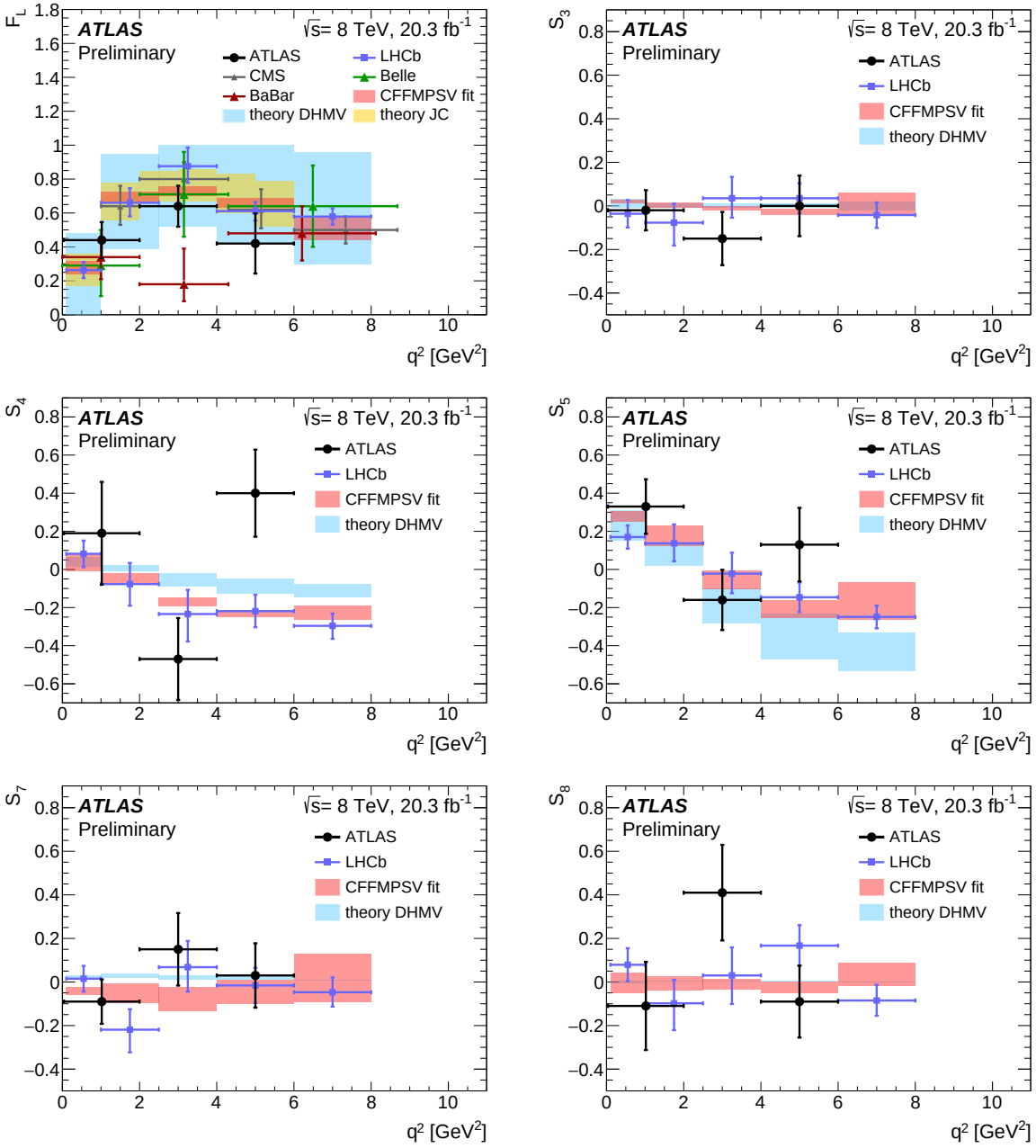

Figure 13: The measured values of F_L, S_3, S_4, S_5, S_7, S_8 compared with predictions from the theoretical groups discussed in the text.

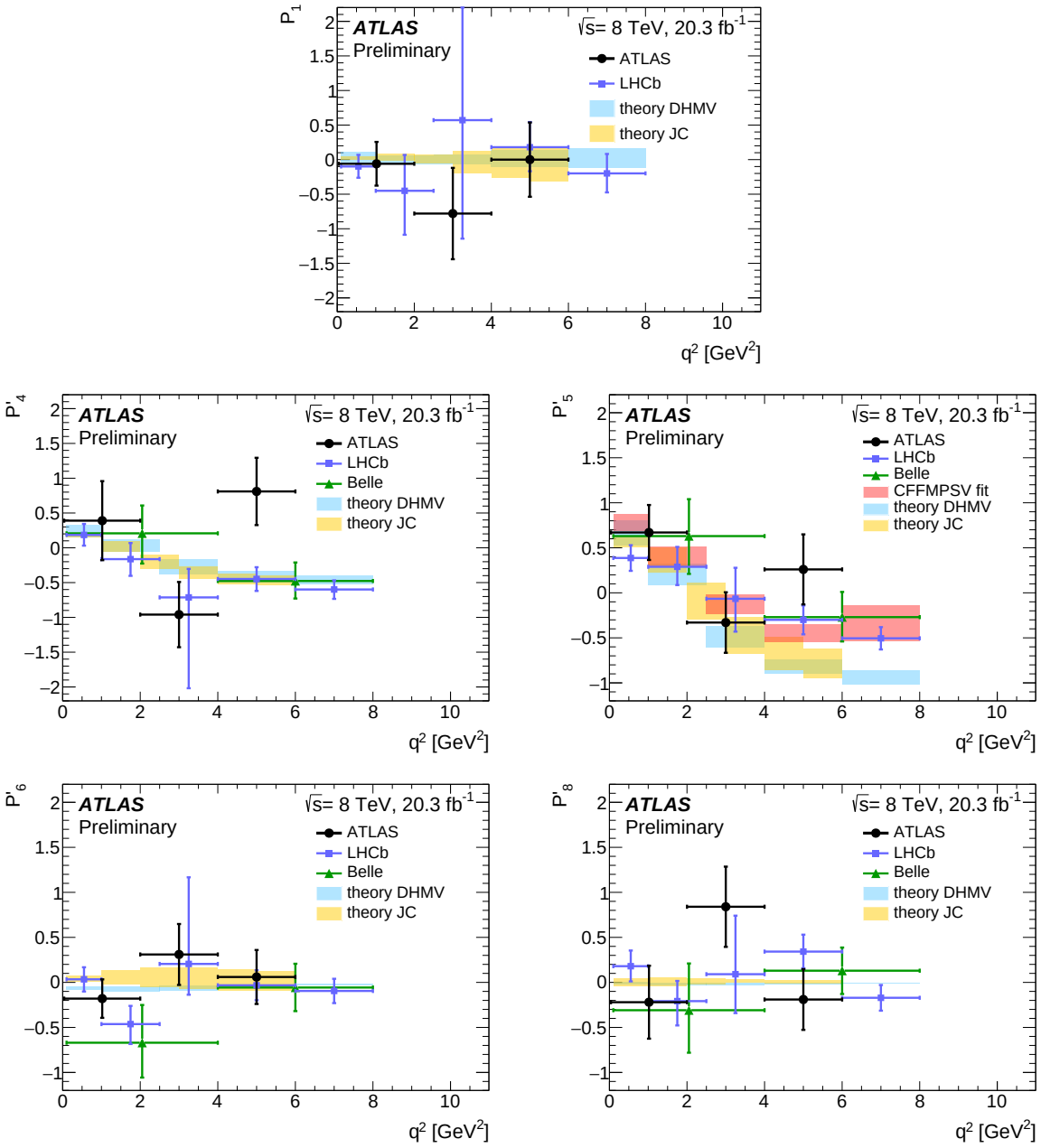

Figure 14: The measured values of P_1, P_4', P_5', P_6', P_8' compared with predictions from the theoretical groups discussed in the text.

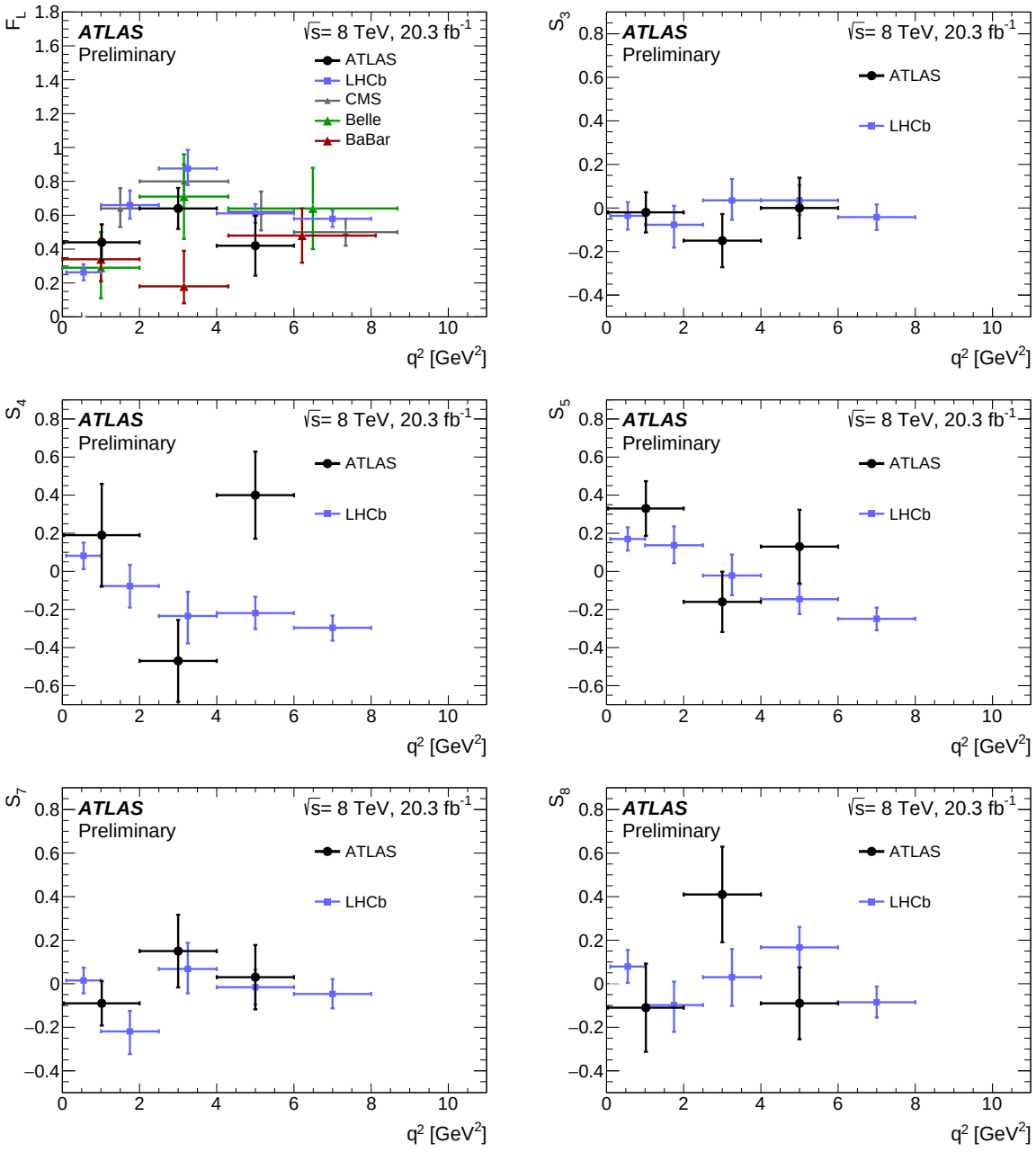

Figure 15: The measured values of F_L, S_3, S_4, S_5, S_7, S_8 compared with results from other experiments.

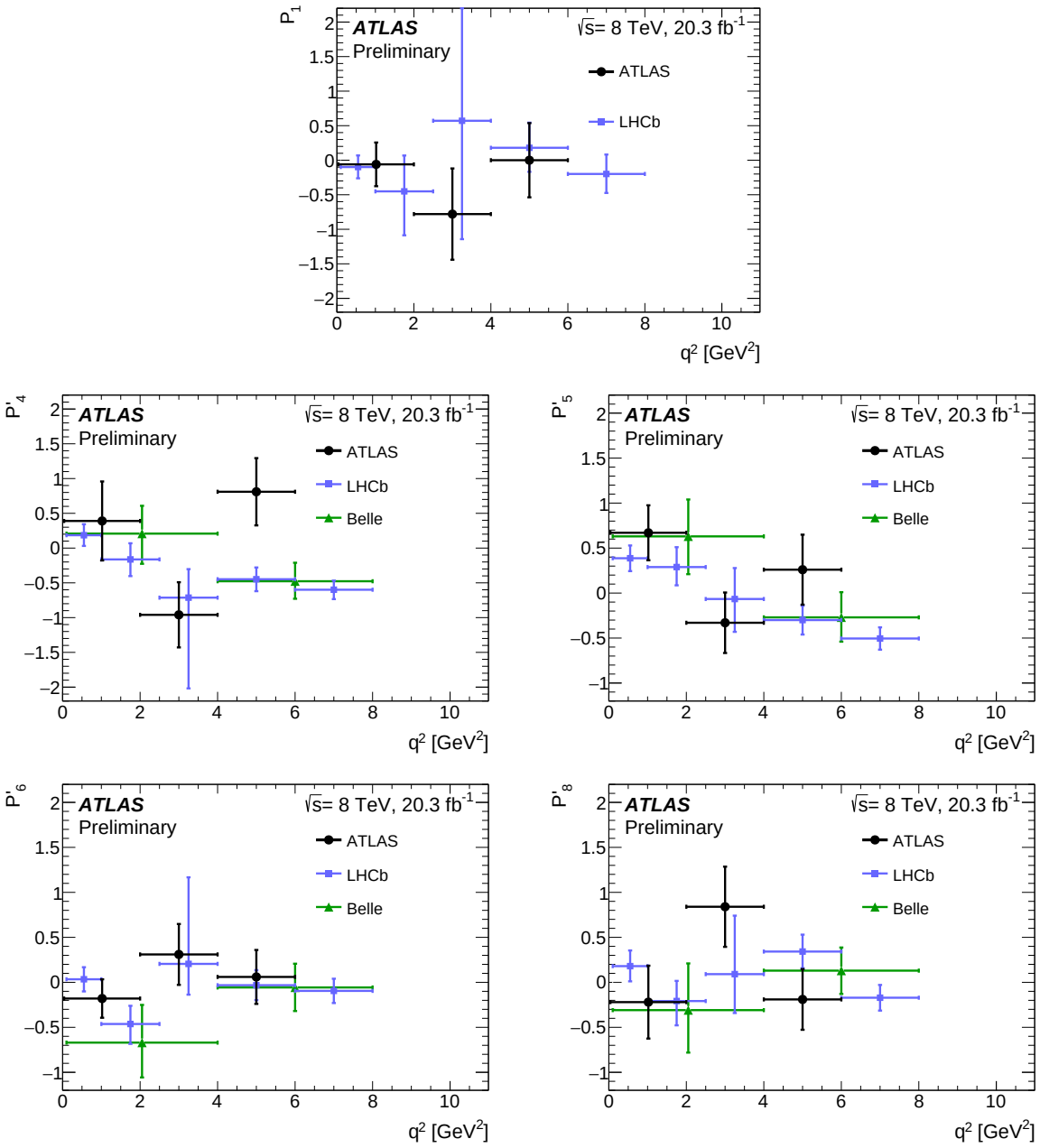

Figure 16: The measured values of P_1, P_4', P_5', P_6', P_8' compared with results from other experiments.

Table 4: The largest value of systematic uncertainties for F_L and S_i from different sources considered. The systematic uncertainties vary from bin to bin in q^2 and some bins have smaller uncertainties than those presented here. Entries marked with − have no contribution from that systematic effect.

Source	F_L	S_3	S_4	S_5	S_7	S_8
Combinatoric $K\pi$ (fake K^*) background	0.03	0.03	0.05	0.03	0.06	0.13
D and B^+ veto	0.11	0.04	0.05	0.03	0.01	0.05
Background p.d.f. shape	0.04	0.04	0.03	0.02	0.03	0.01
Acceptance function	0.01	0.01	0.07	0.01	0.01	0.01
Partially reconstructed decay background	0.03	0.05	0.02	0.06	0.05	0.05
Alignment and B field calibration	0.02	0.04	0.05	0.03	0.04	0.03
Fit bias	0.01	0.01	0.02	0.02	0.01	0.04
Data/MC differences for p_T	0.02	0.02	0.01	0.01	0.01	0.01
S-wave	0.01	0.01	0.01	0.01	0.01	0.02
Nuisance parameters	0.01	0.01	0.01	0.01	0.01	0.01
Λ_b, B^+ and B_s background	0.01	0.01	0.01	0.01	0.01	0.01
Misreconstructed signal	0.01	0.01	0.01	0.01	0.01	0.01
Dilution	–	–	0.01	0.01	–	–

References

[1] Belle Collaboration, J.-T. Wei et al., *Measurement of the Differential Branching Fraction and Forward-Backword Asymmetry for $B \to K^{(*)} l^+ l^-$*, Phys. Rev. Lett. **103** (2009) 171801, arXiv: 0904.0770 [hep-ex].

[2] CDF Collaboration, T. Aaltonen et al., *Measurements of the Angular Distributions in the Decays $B \to K^{(*)} \mu^+ \mu^-$ at CDF*, Phys. Rev. Lett. **108** (2012) 081807, arXiv: 1108.0695 [hep-ex].

[3] LHCb Collaboration, R. Aaij et al., *Measurement of Form-Factor-Independent Observables in the Decay $B^0 \to K^{*0} \mu^+ \mu^-$*, Phys. Rev. Lett. **111** (2013) 191801, arXiv: 1308.1707 [hep-ex].

[4] LHCb Collaboration, R. Aaij et al., *Angular analysis of the $B^0 \to K^{*0} \mu^+ \mu^-$ decay using 3 fb^{-1} of integrated luminosity*, JHEP **02** (2016) 104, arXiv: 1512.04442 [hep-ex].

[5] CMS Collaboration, *Angular analysis of the decay $B^0 \to K^{*0} \mu^+ \mu^-$ from pp collisions at $\sqrt{s}$ = 8 TeV*, Phys. Lett. B **753** (2016) 424, arXiv: 1507.08126 [hep-ex].

[6] BaBar Collaboration, J. P. Lees et al., *Measurement of angular asymmetries in the decays $B \to K^* \ell^+ \ell^-$*, Phys. Rev. D **93** (2016) 052015, arXiv: 1508.07960 [hep-ex].

[7] Belle Collaboration, S. Wehle et al., *Lepton-Flavor-Dependent Angular Analysis of $B \to K^* \ell^+ \ell^-$*, (2016), arXiv: 1612.05014 [hep-ex].

[8] LHCb Collaboration, R. Aaij et al., *Differential branching fraction and angular analysis of the decay $B^0 \to K^{*0} \mu^+ \mu^-$*, JHEP **08** (2013) 131, arXiv: 1304.6325.

[9] L. Evans and P. Bryant, *LHC Machine*, JINST **3** (2008) S08001.

[10] K. G. Wilson and W. Zimmermann, *Operator product expansions and composite field operators in the general framework of quantum field theory*, Commun. Math. Phys. **24** (1972) 87.

[11] W. Altmannshofer and D. M. Straub, *New physics in $B \to K^* \mu\mu$?*, Eur. Phys. J. C **73** (2013) 2646, arXiv: 1308.1501 [hep-ph].

[12] S. Descotes-Genon, L. Hofer, J. Matias and J. Virto, *Global analysis of $b \to s\ell\ell$ anomalies*, JHEP **06** (2016) 092, arXiv: 1510.04239 [hep-ph].

[13] I. Dunietz, H. R. Quinn, A. Snyder, W. Toki and H. J. Lipkin, *How to extract CP violating asymmetries from angular correlations*, Phys. Rev. D **43** (1991) 2193.

[14] S. Descotes-Genon, T. Hurth, J. Matias and J. Virto, *Optimizing the basis of $B \to K^* l^+ l^-$ observables in the full kinematic range*, JHEP **05** (2013) 137, arXiv: 1303.5794 [hep-ph].

[15] S. Descotes-Genon, J. Matias, M. Ramon and J. Virto, *Implications from clean observables for the binned analysis of $B \to K^* \mu^+ \mu^-$ at large recoil*, JHEP **01** (2013) 048, arXiv: 1207.2753 [hep-ph].

[16] ATLAS Collaboration, *The ATLAS Experiment at the CERN Large Hadron Collider*, JINST **3** (2008) S08003.

[17] T. Sjostrand, S. Mrenna and P. Z. Skands, *A brief Introduction to PYTHIA 8.1*, Comput. Phys. Commun. **178** (2008) 852, arXiv: 0710.3820 [hep-ph].

[18] D. J. Lange, *The EvtGen particle decay simulation package*, Nucl. Instrum. Meth. A **462** (2001) 152.

[19] E. Barberio and Z. Was, *PHOTOS: A universal Monte Carlo for QED radiative corrections: version 2.0*, Comput. Phys. Commun. **79** (1994) 291.

[20] S. Agostinelli et al., *GEANT4: A Simulation toolkit*, Nucl. Instrum. Meth. A **506** (2003) 250.

[21] ATLAS Collaboration, *The ATLAS Simulation Infrastructure*, Eur. Phys. J. C **70** (2010) 823, arXiv: 1005.4568 [hep-ex].

[22] ATLAS Collaboration, *Measurement of the muon reconstruction performance of the ATLAS detector using 2011 and 2012 LHC proton–proton collision data*, Eur. Phys. J. C **74** (2014) 3130, arXiv: 1407.3935 [hep-ex].

[23] ATLAS Collaboration, *Measurement of the CP-violating phase ϕ_s and the B_s^0 meson decay width difference with $B_s^0 \to J/\psi\phi$ decays in ATLAS*, JHEP **08** (2016) 147, arXiv: 1601.03297 [hep-ex].

[24] A. Ali, P. Ball, L. T. Handoko and G. Hiller, *A comparative study of the decays $B \to (K, K^*)\ell^+\ell^-$ in standard model and supersymmetric theories*, Phys. Rev. D **61** (2000) 074024, arXiv: 9910221 [hep-ph].

[25] LHCb Collaboration, R. Aaij et al., *Measurements of the S-wave fraction in $B^0 \to K^+\pi^-\mu^+\mu^-$ decays and the $B^0 \to K^*(892)^0\mu^+\mu^-$ differential branching fraction*, JHEP **11** (2016) 047, arXiv: 1606.04731 [hep-ex].

[26] M. Ciuchini et al., *$B \to K^*\ell^+\ell^-$ decays at large recoil in the Standard Model: a theoretical reappraisal*, JHEP **06** (2016) 116, arXiv: 1512.07157 [hep-ph].

[27] S. Descotes-Genon, L. Hofer, J. Matias and J. Virto, *On the impact of power corrections in the prediction of $B \to K^*\mu^+\mu^-$ observables*, JHEP **12** (2014) 125, arXiv: 1407.8526 [hep-ph].

[28] S. Jäger and J. Martin Camalich, *On $B \to V\,l\,l$ at small dilepton invariant mass, power corrections, and new physics*, JHEP **05** (2013) 043, arXiv: 1212.2263 [hep-ph].

[29] S. Jäger and J. Martin Camalich, *Reassessing the discovery potential of the $B \to K^*\ell^+\ell^-$ decays in the large-recoil region: SM challenges and BSM opportunities*, Phys. Rev. D **93** (2016) 014028, arXiv: 1412.3183 [hep-ph].